Surface Debye temperatures of rhodium (100) and (111) surfaces

D. G. Castner* and G. A. Somorjai
Materials and Molecular Research Division, Lawrence Berkeley Laboratory, and Department of Chemistry, University of California, Berkeley, Berkeley, California 94720

J. E. Black,† D. Castiel,‡ and R. F. Wallis
Department of Physics, University of California, Irvine, Irvine, California 92717
(Received 6 April 1981)

Surface Debye temperatures have been measured for rhodium (100) and (111) surfaces using a conventional low-energy-electron-diffraction–Auger-electron-spectroscopy system. The 00 beam intensities were measured with a spot photometer and the crystal temperature was monitored with a Pt versus Pt–10 at. % Rh thermocouple. From the intensity versus temperature curve, a Debye temperature was calculated for each beam voltage. The surface Debye temperatures were then estimated from plots of Debye temperature versus beam voltage. Using three-constant and five-constant lattice-dynamical models, we have made calculations of the bulk phonon dispersion curves and the surface Debye temperatures. A comparison is given of the experimental and theoretical results for the surface Debye temperatures.

I. INTRODUCTION

The experimental technique of low-energy-electron diffraction (LEED) has proven to be very useful for the study of surface structures and surface vibrational properties of crystals. In the present paper we are particularly interested in the determination of the mean-square displacement (MSD) of a surface atom through LEED.[1] To measure the MSD experimentally at solid surfaces, one can observe the intensity of elastically backscattered low-energy electrons as a function of temperature and energy. The MSD is then extracted from the Debye-Waller factors of the Bragg peaks at the lowest energies.

In this paper, we report both experimental and theoretical results for the ratio of the surface MSD to the bulk MSD for the (100) and (111) surfaces of the face-centered-cubic crystal rhodium. The experimental values were obtained from the temperature dependence of Bragg peaks in LEED. The theoretical calculations were carried out using two lattice-dynamical models involving three force constants and five force constants, respectively. Changes in the surface force constants from their bulk value are neglected. Our theoretical results are compared with the experimental results reported in this paper and with those of Chan *et al.*,[2] who used LEED to determine the surface Debye temperature of the (111) surface of rhodium.

II. EXPERIMENTAL

The samples were prepared by orienting a rhodium single-crystal rod of > 99.9% purity to within ± 0.5° and then using spark erosion to cut (111) and (100) slices 1 mm thick and 7 mm in diameter. After mechanical polishing and etching, the samples were mounted in a modified Varian LEED-Auger apparatus incorporating a Varian four-grid LEED optics which also served as the Auger analyzer. A 2.5-keV grazing-incidence electron gun was used to stimulate Auger emission. Base pressures of 5×10^{-10} Torr were routinely obtained.

Cleaning in vacuum was accomplished by a combination of ion bombardment (500–2000 eV), annealing, and O_2 and H_2 cycles to remove carbon, sulfur, phosphorus, and boron. After cleaning, no carbon, sulfur, or phosphorus could be detected by Auger electron spectroscopy (AES). Boron, a significant bulk impurity (17 ppm), segregated onto both surfaces and could be detected by its ordered LEED structures and a 180-eV peak in the AES spectrum. Ion bombardment (500 eV) at 300 K followed by a 675-K anneal *in vacuo* was found to be a good method of temporarily removing boron from both faces. As boron was depleted from the bulk, it ceased segregating to the surface.

The LEED apparatus was used to determine experimental values of the Debye temperatures Θ_D for the (111) and (100) surfaces of rhodium. The LEED patterns of the clean Rh (111) and (100) surfaces show the (1×1) symmetry characteristic of the unreconstructed clean surfaces. These LEED patterns have sharp intense spots and low background intensity. The intensity versus voltage (I-V) curves for the 00 diffraction beams from these two surfaces are shown in Fig. 1. The diffraction beam intensities were measured with a spot photometer. To select the Bragg peaks and determine the inner potential V_0 and topmost

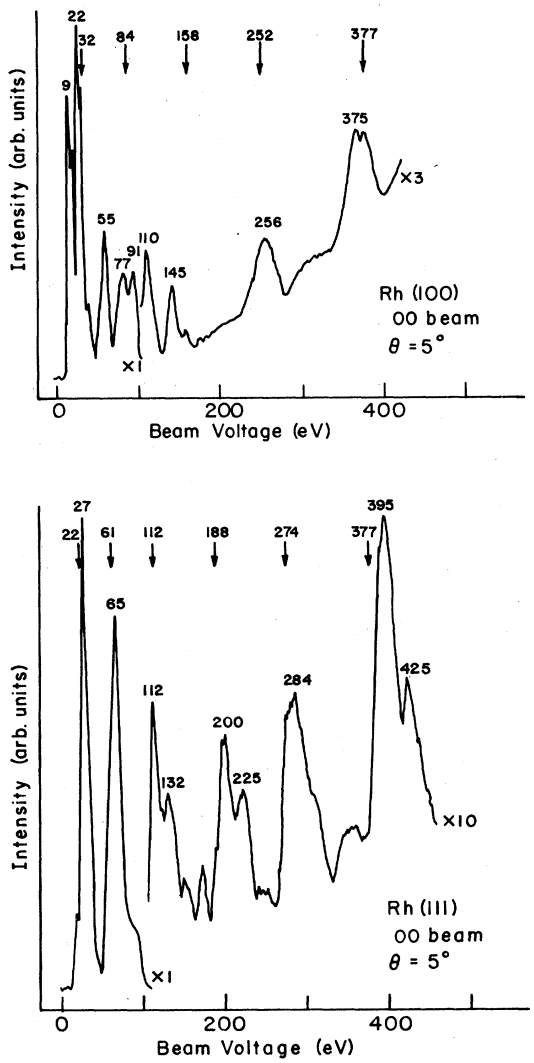

FIG. 1. *I-V* curves for the rhodium (111) and (100) specular diffraction beams.

interlayer spacing c, the following equation was employed, which relates the incident electron energy E (in eV) to the peak index l and the angle θ between the incident direction and the normal to the surface:

$$E=\frac{150.4}{4c^2\cos^2\theta}l^2-\frac{V_0}{\cos^2\theta}\,. \tag{2.1}$$

First, the energies at which the Bragg peaks are expected to occur are determined using the bulk interlayer spacing and $V_0=10$ eV, typical values for most metals. These calculated energies are then matched to the experimental energies as shown in Tables I and II. Bragg peaks are generally the major peaks in an *I-V* profile and this fact can be used as a guide in separating the Bragg peaks from the multiple scattering peaks. For the Rh(111) surface the separation is straightforward because the *I-V* profile is nearly kinematical. The *I-V* profile from the Rh(100) surface has several large multiple scattering peaks below 125 eV, making the Bragg peak assignment more difficult in this region. Either the 77- or 91-eV peaks could be taken as the $l=3$ Bragg peak. On the basis of the Θ_D calculations the 77-eV peak was taken as the Bragg peak. This will be discussed below in further detail. After the Bragg assignments have been made, experimental values for c and V_0 are calculated from the slope and intercept of the straight line drawn through the E_{expt} vs l^2 data points. The results obtained from the data in Tables I and II are summarized in Table III. The slight contraction of the surface layer is smaller than the experimental error; therefore, within the accuracy of these calculations the rhodium (111) and (100) surfaces are unrelaxed. Multiple scattering calculations have shown that Δc is between -3% and 0% and V_0 ranges between 10.7 and 11.5 eV on the rhodium (111), (100), and (110) surfaces.[3-6] Thus the kinematical and multiple scattering calculations are in very good agreement.

A determination of Θ_D was made for each of the Bragg peaks listed in Tables I and II. An intensity versus temperature profile at $\theta=5°$ for the specular $l=7$ Bragg peak from the Rh(111) surface is shown in Fig. 2. The other Bragg peaks had similar profiles. These profiles were obtained by

TABLE I. Selection of the Bragg peaks for Rh(111).

l	l^2	E_{calc} (eV)[a]	E_{expt} (eV)
1	1		
2	4	22	27
3	9	61	65
4	16	112	112
5	25	188	200
6	36	274	284
7	49	377	395

[a] Values of $V_0=10$ eV and $c=2.19$ Å were used to determine E_{calc} from Eq. (2.1).

TABLE II. Selection of the Bragg peaks for Rh(100).

l	l^2	E_{calc} (eV)[a]	E_{expt} (eV)
1	1		
2	4	32	22
3	9	84	77
4	16	158	145
5	25	252	256
6	36	368	375

[a] Values of $V_0=10$ eV and $c=1.90$ Å were used to determine E_{calc} from Eq. (2.1).

TABLE III. Calculation of the topmost interlayer spacing and inner potential for Rh(111) and Rh(100).

Crystal face	Slope	c_{expt} (Å)	c_{bulk} (Å)	Δc $\left(\frac{c_{expt}-c_{bulk}}{c_{bulk}}\times 100\right)$	Intercept	V_0 (eV)
Rh(111)	8.23	2.15	2.19	−2%	−10	10
Rh(100)	10.9	1.86	1.90	−2%	−11	11

monitoring the intensity of a given Bragg peak with a spot photometer as the crystal cooled from 800 °C to 50 °C. The crystal was then rotated back to $\theta = 0°$ and the background intensity was measured in the same manner. The intensities were monitored during cooling instead of heating to avoid distortions from the heating currents. The values of I_{00} (Bragg peak intensity), I_{bkgd} (background intensity), $I_{00}^* = I_{00} - I_{bkgd}$, and $\ln I_{00}^*$ for the curves in Fig. 2 have been tabulated in Table IV. The plot of $\ln I_{00}^*$ versus temperature of these values shown in Fig. 3 yields a straight line with a slope of -5.14×10^{-3}. Using this slope the Debye temperature was calculated using the equation

$$\ln I = \frac{0.153E}{M\Theta_D^2}T + b\,, \tag{2.2}$$

where E is the electron energy including the inner potential, M is the atomic mass, T is the absolute temperature, and b is the natural logarithm of the atomic structure factor. The result is $\Theta_D = 340$ K. The values of Θ_D for the other Bragg peaks were calculated in a similar manner. The results of these calculations are shown in Fig. 4. These values are the average of several experiments. Since only the 00 beam was used, the Debye temperatures refer to the component of displacement normal to the surface. The estimated errors in Θ_D arose from noise in the intensity measurements and difficulty in making an accurate measurement of the beam voltage. A value of Θ_D was also calculated for the 91-eV peak on Rh(100), but this value deviated significantly from the curve shown in Fig. 4. For this reason the 77-eV peak was selected as the $l = 3$ Bragg peak for the Rh(100) surface.

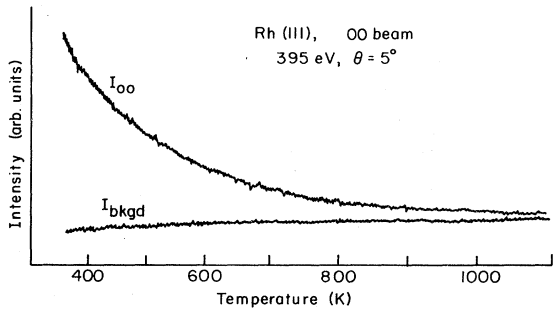

FIG. 2. Intensity vs temperature curves for the specular $l = 7$ Bragg peak from rhodium (111), I_{00}, and the background intensity from rhodium (111), I_{bkgd}.

Considering first the data for the (100) surface in Fig. 4, we see that the apparent Debye temperature decreases monotonically with decreasing beam voltage. Extrapolation of the data to zero beam voltage yields the "zero-penetration" surface Debye temperature of ~200 K. Turning now to the (111) surface, we observe that the apparent Debye temperature decreases with decreasing beam voltage until a minimum is reached at about 100 eV, after which it increases with further decrease in the beam voltage. This behavior is anomalous and may be an artifact of the particular experimental arrangement used. If the minimum is ignored and the curve is extrapolated linearly to zero beam voltage, a zero-penetration surface Debye temperature of ~210 K is obtained, which is in reasonable agreement with the value of 197 K obtained by Chan *et al.*[2]

The values of Θ_D at the highest beam voltage on each surface are very close to the bulk Θ_D of 350 K determined from specific-heat data[7] at 298 K. Using this value together with the values of the

TABLE IV. Intensity values (arbitrary units) for the curves shown in Fig. 2.

Temperature (K)	I_{00}	I_{bkgd}	I_{00}^*	$\ln I_{00}^*$
353	3.63	0.74	2.89	1.06
394	3.13	0.78	2.35	0.85
432	2.79	0.81	1.98	0.68
468	2.46	0.82	1.64	0.49
503	2.22	0.84	1.38	0.32
537	2.02	0.85	1.17	0.16
582	1.79	0.87	0.92	−0.08
625	1.61	0.88	0.73	−0.31
667	1.47	0.89	0.58	−0.54
708	1.35	0.89	0.46	−0.78
749	1.27	0.90	0.37	−0.99
800	1.19	0.90	0.29	−1.24
850	1.13	0.91	0.22	−1.51
899	1.09	0.91	0.18	−1.71
947	1.07	0.92	0.15	−1.90
1041	1.03	0.93	0.10	−2.30

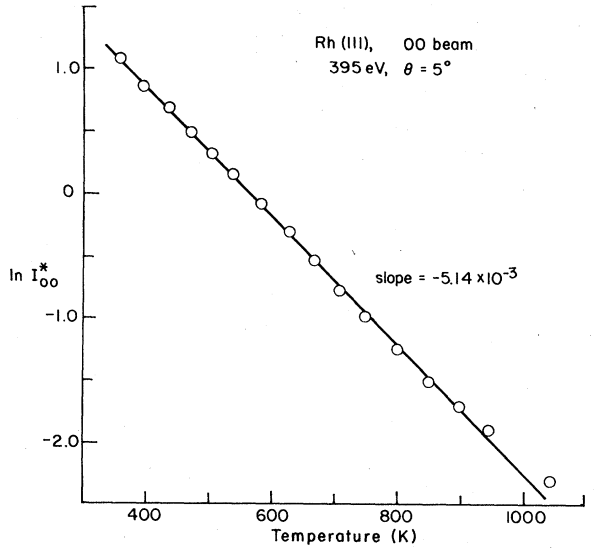

FIG. 3. A plot of $\ln I_{00}^{*}$ vs temperature for the specular $l=7$ Bragg peak from the rhodium (111) surface.

surface Debye temperatures, we can calculate the ratio of the normal components of the surface and bulk mean-square displacements. The results for $\langle u^2\rangle_{\text{surf}}/\langle u^2\rangle_{\text{bulk}}$ are 3.33 and 3.06 for the (111) and (100) surfaces, respectively.

III. LATTICE-DYNAMICAL MODELS

We employ two rotationally invariant lattice-dynamical models. In the first model, we assume central forces between nearest neighbors and next-nearest neighbors and, in addition, angle-bending interactions involving triplets of nearest neighbors. This model contains three force constants and will be referred to as the "three-constant model." In the second model, we assume central potentials of interaction between nearest neighbors and next-nearest neighbors as well as the angle-bending interactions. This model contains five force constants and will be referred to as the "five-constant model." Since the three-constant model can be regarded as a special case of the five-constant model, we shall present the latter in detail and then show how the former is obtained from the latter.

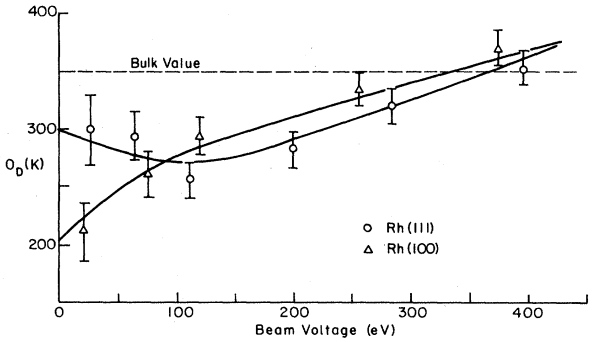

FIG. 4. Values of Θ_D vs beam voltage for the specular Bragg peaks from rhodium (111) and (100) surfaces.

Let us designate the interaction potentials for nearest neighbors and next-nearest neighbors by $\varphi_1(r)$ and $\varphi_2(r)$, respectively, and the position vector of a lattice site by

$$\vec{R}(lmn)=(a_0/2)(l\hat{x}+m\hat{y}+n\hat{z})\,, \tag{3.1}$$

where l, m, and n are integers such that $l+m+n$ is even, a_0 is the fundamental cube edge, and $\hat{x}$, $\hat{y}$, and $\hat{z}$ are unit vectors in the x, y, and z directions, respectively. The equation of motion corresponding to the x component of force can be written as

$$\begin{aligned}M\ddot{u}_{lmn}=\alpha_1&\Big(\sum_{\lambda,\mu=\pm1}(u_{l+\lambda,m+\mu,n}-u_{lmn})+\sum_{\lambda,\nu=\pm1}(u_{l+\lambda,m,n+\nu}-u_{lmn})\Big)+\alpha_2\Big(\sum_{\lambda,\mu=\pm1}\lambda\mu v_{l+\lambda,m+\mu,n}+\sum_{\lambda,\nu=\pm1}\lambda\nu w_{l+\lambda,m,n+\nu}\Big)\\&+\alpha_3\sum_{\mu,\nu=\pm1}(u_{l,m+\mu,n+\nu}-u_{lmn})+\beta_1\sum_{\lambda=\pm2}(u_{l+\lambda,m,n}-u_{lmn})+\beta_2\Big(\sum_{\mu=\pm2}(u_{l,m+\mu,n}-u_{lmn})+\sum_{\nu=\pm2}(u_{l,m,n+\nu}-u_{lmn})\Big)\\&+\gamma\sum_{\lambda,\mu,\nu=\pm1}\left[\tfrac{3}{2}(u_{l+\lambda,m+\mu,n}+u_{l+\lambda,m,n+\nu}+u_{l,m+\mu,n+\nu}-3u_{lmn})+\tfrac{3}{4}(\lambda\mu v_{l+\lambda,m+\mu,n}+\lambda\nu w_{l+\lambda,m,n+\nu})\right],\end{aligned} \tag{3.2}$$

where M is the atomic mass, u_{lmn}, v_{lmn}, and w_{lmn} are the x, y, and z components of displacement of the atom at the lattice site (lmn),

$$\alpha_1=\tfrac{1}{2}[\varphi_1''(r_0)+(1/r_0)\varphi_1'(r_0)]\,, \tag{3.3a}$$

$$\alpha_2=\tfrac{1}{2}[\varphi_1''(r_0)-(1/r_0)\varphi_1'(r_0)]\,, \tag{3.3b}$$

$$\alpha_3=\alpha_1-\alpha_2\,, \tag{3.3c}$$

$$\beta_1=\varphi_2''(a_0)\,, \tag{3.3d}$$

$$\beta_2=(1/a_0)\varphi_2'(a_0)\,, \tag{3.3e}$$

γ is the force constant associated with angle-bending interactions, and r_0 is the nearest-neighbor equilibrium distance. Two other equations of motion are obtained by cyclically permuting u, v, w and λ, μ, ν.

There seem to be no phonon dispersion curves for rhodium determined by inelastic neutron scattering. We must therefore use other experimental data to determine the force constants. The data which we have been able to locate are the bulk

Debye temperature from specific-heat data,[7] $\Theta_D = 350$ K, the bulk modulus,[8] $B = 2.71 \times 10^{12}$ dyn/cm^2, and the speed of shear sound waves,[9] $c_t = 3.005 \times 10^5$ cm/sec. This gives us three pieces of information, but there are five independent force constants to be determined, so we need two more relationships. One of these is provided by the condition for static equilibrium of the lattice with respect to homogeneous expansions or contractions. This yields

$$2^{1/2}\varphi_1'(r_0) + \varphi_2'(a_0) = 0\,, \tag{3.4}$$

which, using Eqs. (3.3), becomes

$$\alpha_1 - \alpha_2 + \beta_2 = 0\,. \tag{3.5}$$

To get the last relationship needed, we argue that rhodium is very similar in its properties to platinum and palladium. If we examine the elastic constants of these two materials,[10,11] we find that the values of the ratio c_{12}/c_{11} are 0.72 and 0.78, respectively. We take this ratio for rhodium to be the average of these two values—namely, 0.75.

The elastic constants can now be determined using the relation $c_{12} = 0.75 c_{11}$ and the relations

$$B = (c_{11} + 2c_{12})/3\,, \tag{3.6}$$

$$c_{44} = \rho c_t^2\,, \tag{3.7}$$

where ρ is the density having the value[12] 12.4 g/cm^3. The results are, in dyn/cm^2,

$$c_{11} = 3.25 \times 10^{12}\,, \tag{3.8a}$$

$$c_{12} = 2.44 \times 10^{12}\,, \tag{3.8b}$$

$$c_{44} = 1.12 \times 12^{12}\,. \tag{3.8c}$$

By passing to the continuum limit of the equations of motion and comparing the result with the equations of elasticity theory, one can obtain the relations between the force constants and the elastic constants. They are

$$c_{11} = (4\alpha_1 + 4\beta_1 + 12\gamma)/a_0\,, \tag{3.9a}$$

$$c_{12} = (6\alpha_2 - 4\alpha_1 - 4\beta_2 - 6\gamma)/a_0\,, \tag{3.9b}$$

$$c_{44} = (4\alpha_1 - 2\alpha_2 + 4\beta_2 + 12\gamma)/a_0\,. \tag{3.9c}$$

Note that if we ignore the angular interactions by setting $\gamma = 0$ and use Eq. (3.5), we obtain Cauchy's relation, $c_{12} = c_{44}$. Since the latter is not well obeyed, the angular interactions must be important.

The fifth equation needed to specify the force constants concerns the Debye temperature which is ordinarily related to the maximum phonon frequency of the crystal by the equation

$$\hbar\omega_{\max} = k_B\Theta_D\,. \tag{3.10}$$

In actual fact, this relationship is not valid for many materials. For platinum, whose maximum frequency is at the Brillouin-zone boundary in the [111] direction,[13] one finds that

$$k_B\Theta_D = 0.829\hbar\omega_{\max}(111)\,. \tag{3.11}$$

If we assume such a relation for rhodium, we do not get consistent results for the force constants. However, satisfactory results are obtained if we use the maximum frequency in the [100] direction and employ the same relation that is valid for platinum—namely,

$$k_B\Theta_D = 0.836\hbar\omega_{\max}(100)\,. \tag{3.12}$$

It will be seen below that

$$M\omega_{\max}^2(100) = 16\alpha_1 + 48\gamma\,, \tag{3.13}$$

so substitution of Eq. (3.13) into Eq. (3.12) yields

$$M(k_B\Theta_D/\hbar)^2 = 0.699(16\alpha_1 + 48\gamma)\,. \tag{3.14}$$

Equations (3.5), (3.9), and (3.14) can now be solved for the force constants. The results are (in units of 10^4 dyn/cm) $\alpha_1 = 4.06$, $\alpha_2 = 3.80$, $\beta_1 = -0.14$, $\beta_2 = -0.26$, and $\gamma = -0.279$.

The three-constant model arises if we set $\alpha_1 = \alpha_2 = \alpha$, $\beta_1 = \beta$, and $\beta_2 = 0$. The central force constants α and β together with the angle-bending force constant γ are the three independent force constants. They are determined from Eqs. (3.9b), (3.9c), and (3.11). Again borrowing from results to follow, we find that Eq. (3.11) becomes

$$M(k_B\Theta_D/\hbar)^2 = 0.69(16\alpha + 4\beta + 48\gamma)\,. \tag{3.15}$$

Solving for the force constants yields (in units of 10^4 dyn/cm) $\alpha = 3.80$, $\beta = 1.23$, and $\gamma = -0.279$.

IV. PHONON DISPERSION CURVES

The phonon dispersion curves are readily determined by substituting plane-wave solutions into the equations of motion. Let

$$(u, v, w)_{lmn} = (U, V, W)\exp[i(l\varphi_1 + m\varphi_2 + n\varphi_3) - i\omega t]\,, \tag{4.1}$$

where U, V, and W are constant amplitudes, the φ_i are dimensionless components of the wave vector, and ω is the frequency. If we substitute Eq. (4.1) into the equations of motion as typified by Eq. (3.2) and set the determinant of the coefficients of U, V, and W equal to zero, we obtain the secular equation

$$|D_{ii'}| = 0, \tag{4.2}$$

where

$$D_{ii} = 4\alpha_1(2 - C + C_jC_k) + 4(\alpha_1 - \alpha_2)(1 - C_jC_k) + 2\beta_1(1 - C_i') + 2\beta_2(2 - C_j' - C_k') + 12\gamma(3 - C) - M\omega^2, \tag{4.3a}$$

$$D_{ii'} = (4\alpha_2 + 6\gamma)S_iS_{i'}, \quad i' \neq i, \tag{4.3b}$$

$C_i = \cos\varphi_i$, $S_i = \sin\varphi_i$, $C_i' = \cos 2\varphi_i$, $C = C_1C_2 + C_2C_3 + C_1C_3$, $i = 1$, 2, or 3, and j and k are the values in the triad (1, 2, 3) which are not equal to i.

The secular equation can be solved analytically for phonons propagating along principal directions in wave-vector space. The following results are obtained for the squared phonon frequencies:

(a) [100] direction, $\varphi_1 = \varphi$, $\varphi_2 = \varphi_3 = 0$:

$$\omega_L^2(\varphi, 0, 0) = (1/M)[(16\alpha_1 + 48\gamma)\sin^2(\varphi/2) + 4\beta_1 \sin^2\varphi], \tag{4.4a}$$

$$\omega_T^2(\varphi, 0, 0) = (1/M)[(16\alpha_1 - 8\alpha_2 + 48\gamma)\sin^2(\varphi/2) + 4\beta_2 \sin^2\varphi]. \tag{4.4b}$$

(b) [110] direction, $\varphi_1 = \varphi_2 = \varphi$, $\varphi_3 = 0$:

$$\omega_L^2(\varphi, \varphi, 0) = (1/M)[(16\alpha_1 - 8\alpha_2 + 48\gamma)\sin^2(\varphi/2) + (4\alpha_1 + 4\alpha_2 + 4\beta_1 + 4\beta_2 + 18\gamma)\sin^2\varphi], \tag{4.5a}$$

$$\omega_{T_1}^2(\varphi, \varphi, 0) = (1/M)[(16\alpha_1 - 8\alpha_2 + 48\gamma)\sin^2(\varphi/2) + (4\alpha_1 - 4\alpha_2 + 4\beta_1 + 4\beta_2 + 6\gamma)\sin^2\varphi], \tag{4.5b}$$

$$\omega_{T_2}^2(\varphi, \varphi, 0) = (1/M)[(16\alpha_1 + 48\gamma)\sin^2(\varphi/2) + (4\alpha_1 - 4\alpha_2 + 8\beta_2 + 12\gamma)\sin^2\varphi]. \tag{4.5c}$$

(c) [111] direction, $\varphi_1 = \varphi_2 = \varphi_3 = \varphi$:

$$\omega_L^2(\varphi, \varphi, \varphi) = (1/M)(12\alpha_1 + 4\alpha_2 + 4\beta_1 + 8\beta_2 + 48\gamma)\sin^2\varphi, \tag{4.6a}$$

$$\omega_T^2(\varphi, \varphi, \varphi) = (1/M)(12\alpha_1 - 8\alpha_2 + 4\beta_1 + 8\beta_2 + 30\gamma)\sin^2\varphi. \tag{4.6b}$$

The phonon dispersion curves calculated from the three-constant and five-constant models are shown in Fig. 5. The two models give qualitatively similar results. An interesting difference, however, is the relative order of the maximum frequencies in the [100] and [111] directions. For the five-constant model, it is the [100] direction which has the higher maximum frequency, whereas for the three-constant model, it is the [111] direction. The latter is the situation which obtains for platinum,[13] although the difference between the two frequencies is very small.

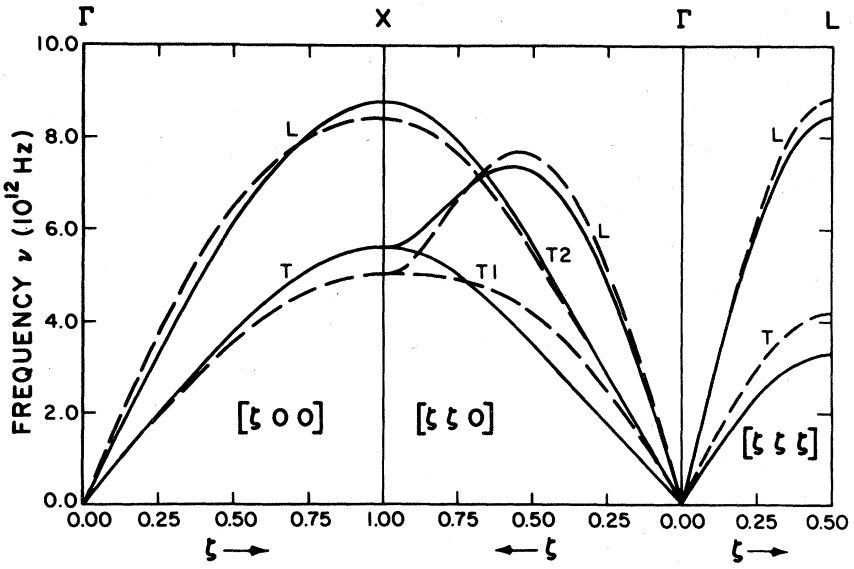

FIG. 5. Theoretical bulk phonon dispersion curves for rhodium. The solid line is the five-constant model and the dashed line is the three-constant model.

V. MEAN-SQUARE DISPLACEMENTS

The mean-square displacements are calculated by applying the method of continued fractions developed by Haydock, Heine, and Kelly[14] for electronic problems and modified for lattice-dynamical problems by Black, Laks, and Mills.[15] We shall only summarize the method and refer the reader to Black *et al.* for details.

The mean-square-displacement component $\langle u_\alpha^2(\vec{l})\rangle$ of an atom at lattice site $\vec{l}$ can be expressed in terms of the eigenvector components $e_\alpha^{(s)}(\vec{l})$ of the dynamical matrix by[1]

$$\langle u_\alpha^2(\vec{l})\rangle = \frac{1}{M}\sum_s |e_\alpha^{(s)}(\vec{l})|^2 \frac{\bar{\epsilon}(\omega_s)}{\omega_s^2}, \tag{5.1}$$

where ω_s is the frequency of the sth normal mode of vibration, $\bar{\epsilon}(\omega_s)$ is the mean phonon energy given by

$$\bar{\epsilon}(\omega_s) = \hbar\omega_s[\bar{n}(\omega_s) + \tfrac{1}{2}], \tag{5.2}$$

and $\bar{n}(\omega_s)$ is the mean phonon occupation number

$$\bar{n}(\omega_s) = \frac{1}{e^{\hbar\omega_s/k_BT} - 1}. \tag{5.3}$$

For a monatomic lattice, the elements of the dynamical matrix $D_{\alpha\beta}(\vec{l},\vec{l}')$ are given by

$$D_{\alpha\beta}(\vec{l},\vec{l}') = \Phi_{\alpha\beta}(\vec{l},\vec{l}')/M, \tag{5.4}$$

where $\Phi_{\alpha\beta}(\vec{l},\vec{l}')$ is the matrix of force constants in Eq. (3.2). In the high-temperature limit, $k_BT \gg \hbar\omega_s$,

$$\bar{n}(\omega_s) \simeq k_BT/\hbar\omega_s, \tag{5.5}$$

and Eq. (5.1) becomes

$$\langle u_\alpha^2(\vec{l})\rangle \simeq \frac{k_BT}{M}\sum_s \frac{|e_\alpha^{(s)}(\vec{l})|^2}{\omega_s^2}. \tag{5.6}$$

Introducing the Green's function

$$U_{\alpha\beta}(\vec{l}\,\vec{l}';z) = \left\langle \vec{l}\alpha \left| \frac{1}{z^2\bar{\bar{1}} - \bar{\bar{D}}} \right| \vec{l}'\beta \right\rangle \tag{5.7}$$

$$= \sum_s \frac{e_\alpha^{(s)}(l) e_\beta^{(s)}(\vec{l}')}{z^2 - \omega_s^2}, \tag{5.8}$$

we see that

$$\langle u_\alpha^2(\vec{l})\rangle \simeq -(k_BT/M)U_{\alpha\alpha}(\vec{l}\,\vec{l};0). \tag{5.9}$$

In the procedure of Haydock *et al.*[14] the Green's function $U_{\alpha\alpha}(\vec{l}\,\vec{l};z)$ as specified by Eq. (5.7) is expanded in the continued fraction

$$U_{\alpha\alpha}(\vec{l}\,\vec{l};z) = \cfrac{1}{z^2 - A_1 - \cfrac{|B_2|^2}{z^2 - A_2 - \cfrac{|B_3|^2}{z^2 - A_3 - \cdots}}}. \tag{5.10}$$

The construction of the coefficients A_i and B_i and the evaluation of the continued fraction are discussed by Black *et al.*[15]

The method just described has been used to calculate the mean-square-displacement components of atoms at the (100) and (111) surfaces and in the bulk of rhodium. From the ratio of the surface and bulk components, one can calculate the ratio of the squares of the surface and bulk Debye temperatures using the relation[1]

$$\frac{\langle u_S^2\rangle}{\langle u_B^2\rangle} = \frac{\Theta_{DB}^2}{\Theta_{DS}^2}, \tag{5.11}$$

which is valid in the high-temperature limit. Knowing the bulk Debye temperature, one can then calculate the surface Debye temperature. The theoretical results for the surface Debye temperatures associated with displacements both parallel and perpendicular to the surface are presented in Table V for the (100) and (111) surfaces of rhodium. The experimental values from this work and from that of Chan *et al.*[2] are also presented.

VI. DISCUSSION

The results shown in Table V for the three-constant and five-constant models are qualitatively rather similar. The perpendicular-surface Debye temperature is about 245 K for both models for the (100) surface and slightly greater for the (111) surface. The parallel-surface Debye temperature is about 300 K or more for both models for both surfaces. Thus, the anisotropy of the mean-square displacements at each surface is clearly evident.

Experimental data are available only for the perpendicular component ratios. We see from Table V that the theoretical values for both surfaces exceed the experimental values by 20% or more. This discrepancy suggests that the force constants coupling a surface atom to its neighbors are significantly smaller than the corresponding force constants in the bulk. The use of the high-temperature limit in our calculations cannot be

TABLE V. Theoretical and experimental values for the surface Debye temperatures at the (100) and (111) surfaces of rhodium.

	(100) surface		(111) surface	
	⊥	∥	⊥	∥
Three-constant model	242	307	247	296
Five-constant model	247	296	261	334
Experiment [a]	200		210	
Experiment [b]			197	

[a] This work.
[b] Reference 2.

responsible for the discrepancy between theory and experiment, since the surface-to-bulk mean-square-displacement ratio decreases rather than increases as the temperature is lowered.

Our experimental result for the surface Debye temperature of the (111) surface is in reasonable agreement with that of Chan *et al.*[2] The difference between the results may be due to the fact that the experiments were done at different azimuthal angles.

In a recent paper, Ernst and Bloch[16] have made an estimate of the surface Debye temperature of rhodium based on an analysis of field emission studies. Since an emitter tip is composed of several different crystallographic surfaces, the results may represent an average over a number of surfaces or may not even refer to a surface at all, but to an edge or a corner. Ernst and Bloch obtain values for the surface Debye temperature in the range of 80–120 K, which are significantly smaller than either the experimental values obtained from LEED or the theoretical values. This suggests that Ernst and Bloch may be dealing with an edge or corner with a high curvature.

ACKNOWLEDGMENTS

The work at the University of California, Berkeley, was supported by the Office of Basic Energy Sciences, Materials Science Division, U. S. Department of Energy, under Contract No. W-7405-ENG-48. The work at the University of California, Irvine, was supported by the Department of Energy under Contract No. DE-AT0379-ER1043 and by the National Science Foundation under Grant No. DMR-7809430.

---

*Present address: Chevron Research Company, 576 Standard Ave., Richmond, California 94802.
†On leave from the Department of Physics, Brock University, St. Catherines, Ontario, Canada, L2S 3A1.
‡ Present address: General Electric Company, 401 N. Washington St., Rockville, Maryland 20850.

[1]See, for example, G. A. Somorjai, *Principles of Surface Chemistry* (Prentice-Hall, Englewood Cliffs, 1972); R. F. Wallis, Prog. Surf. Sci. 4, 233 (1973).
[2]C-M. Chan, P. A. Thiel, J. T. Yates, and W. H. Weinberg, Surf. Sci. 76, 296 (1978).
[3]F. R. Shepherd, P. R. Watson, D. C. Frost, and K. A. R. Mitchell, J. Phys. C 11, 4591 (1978).
[4]K. A. R. Mitchell, F. R. Shepherd, P. R. Watson, and D. C. Frost, Surf. Sci. 64, 737 (1977).
[5]P. R. Watson, F. R. Shepherd, D. C. Frost, and K. A. R. Mitchell, Surf. Sci. 72, 562 (1978).
[6]D. C. Frost, S. Hengrasmee, K. A. R. Mitchell, and P. R. Watson, Surf. Sci. 76, L585 (1978).
[7]K. A. Gschneider, in *Solid State Physics*, edited by H. Ehrenreich, F. Seitz, and D. Turnbull (Academic, New York, 1964), Vol. 16, p. 370.
[8]C. Kittel, *Introduction to Solid State Physics*, 4th ed. (Wiley, New York, 1971), p. 143.
[9]T. E. Owen, Prog. Appl. Mater. Res. 6, 69 (1964).
[10]R. E. MacFarlane, J. A. Rayne, and C. K. Jones, Phys. Lett. 18, 91 (1965).
[11]J. A. Rayne, Phys. Rev. 118, 1545 (1960).
[12]H. M. Trent, D. E. Stone, and R. B. Lindsay, in *American Institute of Physics Handbook* (McGraw-Hill, New York, 1957), p. 2–19.
[13]D. H. Dutton, B. N. Brockhouse, and A. P. Miller, Can. J. Phys. 50, 2915 (1972).
[14]R. Haydock, V. Heine, and M. J. Kelly, J. Phys. C 8, 2591 (1975).
[15]J. E. Black, B. Laks, and D. L. Mills, Phys. Rev. B 22, 1818 (1980).
[16]N. Ernst and J. H. Block, Surf. Sci. 91, L27 (1980).